PERFORMANCE EVALUATION OF EXTERIOR RC BEAM-COLUMN JOINTS WITH ECCENTRICITY

Hung-Jen LEE[1], and Jen-Wen KO[2]

SUMMARY

Cyclic loading response of five reinforced concrete corner beam-column connections with one concentric or eccentric beam framing into a rectangular column in strong or weak direction is reported. The specimen variables are the direction of shear acting on the joint and the eccentricity between the beam and column centerlines. Experimental results show that two joints connecting a beam in strong direction were capable of supporting adjacent beam plastic mechanisms. The other three joints connecting a beam in weak direction, however, exhibited significant damage and loss of strength after beam flexural yielding. Eccentricity between beam and column centerlines had detrimental effects on the strength degradation, energy dissipation capacity, and displacement ductility of the specimens. It was concluded that ACI design procedures for estimating nominal joint shear strength were unconservative for the tested corner connections under lateral loading in weak direction of the column. Valuable information is provided to help further improve the design requirements for eccentric corner beam-column connections.

Keywords: *beam-column connection; corner; eccentric; joint; shear strength.*

INTRODUCTION

Shear failure in beam-column joints leading to collapse of reinforced concrete (RC) buildings has been observed in the past earthquakes. The cause of collapse has been attributed to lack of joint confinement, especially for the exterior and corner beam-column joints without beams framing into all four sides. Since the late-1960s, amounts of experimental investigations on the seismic performance of RC beam-column joints have been extensively studied. The majority of the experimental programs has concentric beam-column connections isolated from a lateral-force-resisting frame at the nearest inflection points in the beams and columns framing into the joint. Since 1976, ACI-ASCE Committee 352 has issued design recommendations for RC beam-column joints. (ACI 352R 1976, 1985) Throughout the years these guidelines evolved into state-of-art reports(ACI 352R 1991, 2002) by integrating results of new experimental programs. Finally, a number of these design recommendations for beam-column connections have been adopted in Chapter 21 of ACI 318 Building Code (2005) for seismic design. It should be noted that the current ACI design provisions are primarily developed from test results of concentric beam-column connections, however, eccentric beam-column connections are common in practice. Relatively few RC eccentric beam-column connections have been tested and reported in the literature to date. (e.g., Joh et al. 1991, Lawrance et al. 1991, Raffaelle and Wight 1995, Chen and Chen 1995, Vollum and Newman 1999, Teng and Zhou 2003, Burak and Wight 2002, Shin and LaFave 2004). To clarify the effect of eccentric beams on the behavior of connections, ACI-ASCE Committee 352 has called for additional research on this topic in the past two decades.

In the early-1990s, Joh et al., (1991) Lawrance et al., (1991) as well as Raffaelle and Wight (1995) totally tested six cruciform eccentric beam-column connections with square columns. Early deterioration of connection strength and ductility was observed in these eccentric specimens. The measured stains in joint hoop

[1] *Assistant Professor, National Yunlin University of Science and Technology, Taiwan, e-mail: hjlee@ce.yuntech.edu.tw*
[2] *Former graduate research assistant, National Yunlin University of Science and Technology, Taiwan*

reinforcement and joint shear deformations on the side near beam centerline were larger than those on the side away from beam centerline. Raffaelle and Wight (1995) suggested a formula of reducing the effective joint width for shear resistance of eccentric joints, and indicated that further study of eccentric beam-column connections with rectangular column is needed.

Eccentric corner beam-column connections were first studied in the late-1990s when Chen and Chen (1995) tested five T-shaped eccentric corner connections, as well as Vollum and Newman (1999) tested 10 corner connections with two (one concentric and one eccentric) beams framing in from two perpendicular directions. Chen and Chen (1995) concluded that eccentric corner connections performed inferior to concentric corner connections, and tapered width beams could eliminate the detrimental effect of eccentric beams. In addition, Vollum and Newman (1999) tested specimens with combined loading in various load paths to investigate the strength and failure modes of eccentric beam-column connections and to verify a previously proposed design method. The researchers concluded that the performance of corner connections improved significantly when joint eccentricity was reduced. It should be noted that the aforementioned corner connections had square columns.

Recently, Teng and Zhou (2002) also tested four cruciform eccentric beam-column connections with rectangular columns in an aspect ratio of 2 or 1.33, and concluded that joint eccentricity slightly reduced the lateral strength and stiffness of the tested specimens. Based on analysis of the tested specimens and previous data from the literature, Teng and Zhou (2002) also proposed an equation for calculating the nominal shear strength of eccentric joints by reducing the effective joint width.

Since floor slabs were typically not included in previous eccentric connection tests, Burak and Wight (2002) as well as Shin and LaFave (2004) tested five eccentric beam-column-slab connections in total. Each subassembly consisted of eccentric edge beams, one concentric transverse beam, floor slabs, and rectangular columns with aspect ratios varied from 1.0 to 1.5. Three specimens of Burak and Wight (2002) were tested under sequential loading in two principal directions in which lateral loading was first applied in the edge beam direction and then in the transverse beam direction. Two specimens of Shin and LaFave (2004) were tested under lateral loading in the direction of edge beam to simulate the behavior of an edge connection in an exterior moment-resisting frame. The researchers reported the damage in the joint region of these eccentric beam-column-slab connections was not as severe as that of previous tests (Joh et al. 1991, Raffaelle and Wight 1995) without floor slabs. Including floor slabs significantly improves the overall performance of eccentric connections and delays the deterioration of the joint stiffness and strength.

Beam-column joints in RC buildings probably subjected to lateral loading in two principal directions during an earthquake. However, current ACI design procedures require that joint shear strength to be evaluated in each direction independently and implicitly assume an elliptical interaction relationship for biaxial loading. It should be noted that only one value of permissible shear stress is selected for a joint according to the effective confinement of the vertical faces of the joint, even though the column cross section is rectangular. Current ACI design procedures consider the effects of column's aspect ratio and eccentric beam on joint shear strength by limiting and reducing the effective joint width. More experimental results are needed to verify the effective joint width in eccentric connections. Therefore, this paper focused on the behavior of eccentric corner connections with rectangular column that have not been verified experimentally.

EXPERIMENTAL PROGRAM

Five RC corner beam-column connections were designed, constructed, and tested under reversed cyclic loading. A T-shaped assembly was chosen to represent the essential components of a corner beam-column connection in a two-way building frame subjected to lateral loading in each principal direction. The primary test variables were the lateral loading directions and the eccentricity between the beam and column centerlines. The effect of transverse beams and floor slabs were neglected to ease construction and testing. Therefore, each subassembly had only one beam framing into one corner column in each principal direction.

Specimen Geometry and Reinforcement

The experimental program were designed using a concrete compressive strength of 30 MPa and typical ASTM A706 deformed reinforcement with specified yield strength of 420 MPa. Cross sections and reinforcing details of five specimens, designated as S0, S50 (S series), W0, W75, and W150 (W series), are shown in Fig. 1. The first character (S or W) of the designation represents one South or West beam framing into the column in Strong or

Weak direction. The later numerals denote the eccentricity between the beam and column centerlines in mm. Thus, two concentric (S0 and W0) and three eccentric (S50, W75, W150) connections were totally tested.

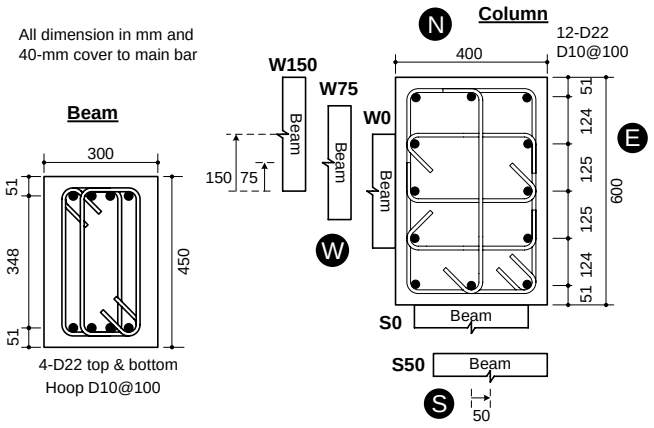

Figure 1 Designation of specimens

The corner column had a cross section of 400x600 mm and used 12 No. 7 (D22) longitudinal bars (gross reinforcement ratio of 1.9%) and No. 3 (D10) hoop with crossties at a spacing of 100 mm throughout the column. The total cross-sectional area of the ties provided in each direction of the column was approximately equal to the minimum amount required in Section 21.4.4.1 of ACI Building Code (2005). To control the input shear force acting on the joint, the loading beam had a cross section of 300x450 mm and used four No. 7 longitudinal bars (steel ratio of 1.29%) at both top and bottom. To avoid beam shear failure and ensure adequate confinement in the plastic hinge region, closed overlapping hoops were also provided through the length of the beam. Fig. 3 illustrates the overall geometry of the specimens. The lengths of the beam and column were chosen to simulate the nearest inflection points in the beam and column framing into the joint.

To avoid anchorage failure and to promote the development of a diagonal compression strut within the joint, the beam longitudinal bars were anchored using a 90-degree standard hook bended into the joint and embedded as close as possible to the back of the column (Fig. 2). Leaving a 70-mm back cover for the tail extension of the hook, the horizontally projected lengths of the hooked beam bars measured form the beam-column interface were 530 mm and 330 mm for S-series and W-series specimens, respectively. The anchorage length of the hooked beam bars in W-series specimens was slightly greater than the development length required in Section 21.5.4.1 of ACI Building Code (2005). In general, five joints were nominally identical except for the joint shear direction, the anchorage length of the hooked beam bar, and the eccentricity between the beam and column centerlines.

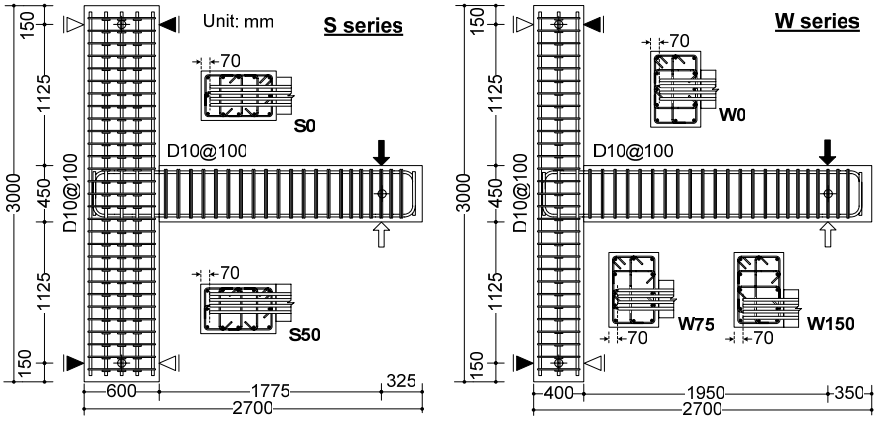

Figure 2 Overall geometry of specimens

Connection Design Parameters

The main design parameters varied in the specimens are listed in Table 1. Due to column bending in strong or weak direction, the ratios of column-to-beam flexural strength (M_r) at the S-series and W-series connections

were equal to 5.10 and 3.46, respectively. Since both M_r values were much greater than the ACI 352 recommend minimum value of 1.4, the flexural hinging in the beam is anticipated. Based on the capacity design concept, the design shear force acting on the joint, V_u, was controlled by the flexural capacity of the beam. For estimating the design joint shear force, a probable strength of $1.25f_y$ for the beam longitudinal reinforcement was included in a strain-compatibility sectional analysis. Due to a little difference on the beam lengths, the design joint shear force was equal to 699 and 706 kN for S-series and W-series specimens, respectively.

The joint shear stress level, γ, was computed using

$$\gamma = \frac{V_u}{\sqrt{f_c'} b_j h_c} \tag{1}$$

where V_u is the design joint shear force; f_c' is the concrete compressive strength; h_c is the column depth in the direction of joint shear to be considered; and b_j is the effective joint width calculated using the following ACI 318 Code (2005) or ACI 352 recommendations (2002).

$$b_j^{318} = \text{the smaller of } \begin{cases} b_b + 2x \\ b_b + h_c \\ b_c \end{cases} \tag{2}$$

$$b_j^{352} = \text{the smaller of } \begin{cases} (b_b + b_c)/2 \\ b_b + \Sigma m h_c/2 \\ b_c \end{cases} \tag{3}$$

where b_b is the beam width; x is the distance between the beam and column edges; b_c is the column width; and m is 0.3 when e is greater than $b_c/8$, otherwise m is 0.5. The joint eccentricity, e, was designed to be $b_c/8$ for specimen S50 and W75, as well as $b_c/4$ for specimen W150.

According to ACI design procedure, the permissible joint shear stress level for corner connections is $1.0\sqrt{f_c'}$ MPa. The γ values reported in Table 1 satisfied the permissible level except for W150 per ACI 318-05 Code. Notably, the design reduction factor of 0.85 is not considered in this paper.

Table 1 Connection design parameters

Specimen	S0	S50	W0	W75	W150
Joint eccentricity e, mm	0	50	0	75	150
Column width b_c, mm	400	400	600	600	600
Column depth h_c, mm	600	600	400	400	400
Moment strength ratio M_r †	5.10	5.10	3.46	3.46	3.46
Effective joint width b_j ‡, mm	400 (350)	300 (350)	600 (450)	450 (450)	300 (360)
Joint shear stress level γ ‡	0.53 (0.61)	0.71 (0.61)	0.54 (0.72)	0.72 (0.72)	1.07 (0.90)

Note: M_r and γ values are computed with $f_c' = 30$ MPa and $f_y = 420$ MPa.

† $M_r = \Sigma M_n(columns)/\Sigma M_n(beams)$.

‡Values outside parentheses are computed using b_j^{318} as per Eq. (2), and values inside parentheses are computed using b_j^{352} as per Eq. (3).

Construction and Material Properties

Two sizes of standard reinforcement meeting ASTM A706 were used for longitudinal and transverse reinforcement in all specimens. The measured yield and ultimate strengths for No. 7 (D22) longitudinal reinforcement were 454.5 and 682.4 MPa, respectively, while yield and ultimate strengths of 471.3 and 715.3 MPa obtained for No. 3 (D10) transverse reinforcement. At least three reinforcing steel coupons were tested for each bar size to get average measured strengths.

Each specimen was cast in a wood form with the beam and column lying on the ground, and the exterior column side (east side for S-series specimens and north side for W-series specimens) faced to the air. Concrete was

supplied by a local ready-mix plant using normal concrete aggregate and placed by pump using a 6-in. diameter hose. Specimen S0 and S50 were cast at one time using a single batch of concrete, and then specimen W0, W75, and W150 were cast in another batch of concrete with the same mix proportions. The fresh concrete was covered with plastic sheets and wet-cured for one week. For each batch of concrete, twelve 150x300-mm concrete cylinders were cast and cured together with the beam-column assemblies. Three cylinders were tested at 28 days and the others were tested on the test day of each beam-column assembly. Table 2 summarizes the concrete compressive strengths at 28 days and the day of assembly test. In addition, average values of test-day concrete strengths were assumed for analytical modeling because the variation in each batch of concrete is not significant.

Table 2 Concrete compressive strengths

Specimen	S0	S50	W0	W75	W150
Concrete batch	1		2		
28-days f_c', MPa	28.5		25.2		
Test days	49	67	53	57	60
Test day f_c', MPa	32.6	34.2	28.9	30.4	29.1
Analytical f_c', MPa	33.2		29.5		

Test Setup and Loading Sequence

Fig. 3 shows the elevation views of the test setup. To restrain the column for a twist about the column axis, each beam-column assembly was rotated 90 degrees and tied down to the strong floor with reaction steel beams, cover plates, and rods. Four one-dimensional rollers seated beside the column to allow in-plane rotation at both ends of the column. This arrangement was chosen to provide stability against torsional action. A column axial load of 700 kN, approximately $0.10A_g f_c'$, was applied using a manually controlled jack and reaction blocks at both ends of the column. Swivel head and base of a servo-controlled actuator were mounted to the beam tip and the reaction wall, respectively. The actuator had a 500-kN load and 750-mm stroke capacity and applied load and displacement to the beam tip. The actuator load was applied at the beam centerline while the column axial load was applied along the column longitudinal axis. For the eccentric beam-column connections, a twist of the column about its longitudinal axis was introduced. More details of other instrumentations can be found in the work by Ko (2005).

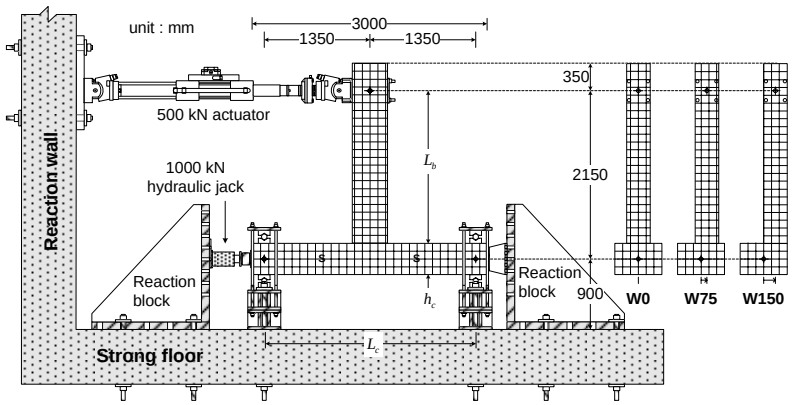

Figure 3 Test setup for W-series specimens (similar setup for S-series specimens)

To simulate the displacement reversal of beam-column connections under earthquake excitations, the specimens were subjected to reversed cyclic lateral displacements. Axial load was applied at the beginning of a test and was held at a level of $0.10A_g f_c'$ during testing. A typical lateral displacement history consisting of three cycles at monotonically increasing drift levels (0.25, 0.50, 0.75, 1.0, 1.5, 2, 3, 4, 5, 6, and 7%) was used for all specimens. The actuator applied each target displacement in a quasi-static manner at a speed ranged from 0.05 to 1.40 mm/s. Target displacement amplitudes at the beam tip, Δ, were computed using the following equation.

$$\text{Drift ratio} = \frac{\delta}{L_c} = \frac{\Delta}{L_b + 0.5h_c} \tag{4}$$

where δ is the inter-story drift of a prototype building frame; L_c is the column height and equal to 2.7 m

between the roller supports at both ends of the column (Fig. 3**)**; $L_b + 0.5h_c$ is the vertical distance between the actuator and column centerlines, and it is equal to 2.15 m for W-series specimens and 2.075 m for S-series specimens (Fig. 2).

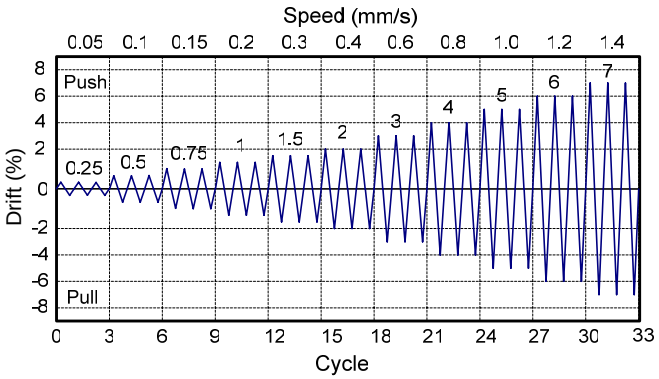

Figure 4 Loading sequence

EXPERIMENTAL RESULTS

Measured response are summarized and discussed in the following subsections. Presented results include: 1) load-displacement response; 2) crack development and failure modes; 3) energy dissipation capacity; 4) steel strain profiles; and 5) joint shear capacity. The results are used to evaluate the influence of joint eccentricity and loading directions on the performance of corner beam-column connections.

Load-Displacement Response

Figure 5 depicts the actuator load-displacement hysteretic curves of for test specimens. The actuator load was normalized to the nominal flexural capacity (P_n) calculated at a given strain of 0.004 for extreme compression fiber of the beam section. The measured material properties were substituted into the constitutive models proposed by Mander et al. (1988) and Priestley et al. (1996) to model the concrete and reinforcing bars, respectively. As shown in Fig. 5, the beam-tip displacement was normalized to story drift ratio and displacement ductility ratio. Using the method in Priestley et al. (1996), the displacement ductility ratio (μ) and nominal yield displacement (Δ_y) are defined as

$$\mu = \frac{\Delta}{\Delta_y} \tag{5}$$

$$\Delta_y = \frac{P_n}{P_{1st\ yield}} \Delta_{1st\ yield} \tag{6}$$

where $P_{1st\ yield}$ and $\Delta_{1st\ yield}$ are actuator load and displacement, respectively, corresponding to the first yielding of the beam longitudinal bar that measured at the beam-column interface.

The measured load-displacement responses for specimen S0 and S50, as shown in Fig. 5, are very similar in stiffness, strength, and ductility. First beam bar yielding was measured during the 1.0% drift cycle and maximum load was recorded at 5% drift level. The hysteretic curves show relatively little pinching which represents typical behavior of systems dominated by flexure. The failure mechanisms for specimen S0 were core concrete crushing and subsequent buckling of longitudinal bar in the beam plastic hinge region. The eccentric specimen S50 had the same failure mechanisms except its earlier buckling of beam bars during the second cycle at 5% drift level. It was concluded that both joints were capable of supporting complete formation of a beam plastic hinge.

As shown in Fig. 5, the load-displacement responses of the W-series specimens were similar up to 4% drift cycle after yielding of beam bars (1% drift) and joint crossties (2% to 3% drift cycle). All three joints were capable of supporting beam flexural yielding up to 4% drift, however, then considerable strength degradation were observed after the maximum loads recorded at 4% (specimen W150) or 5% drift (specimen W0 and W75). The percentage of strength degradation from first to third cycle of 5% drift level was about 10% for specimen W0 and W75, but it was about 30% for specimen W150 at the same drift level. Finally, significant pinching effect shown in Fig. 5 was attributed to the damage of joint region and the slippage of beam bars anchored in the joint.

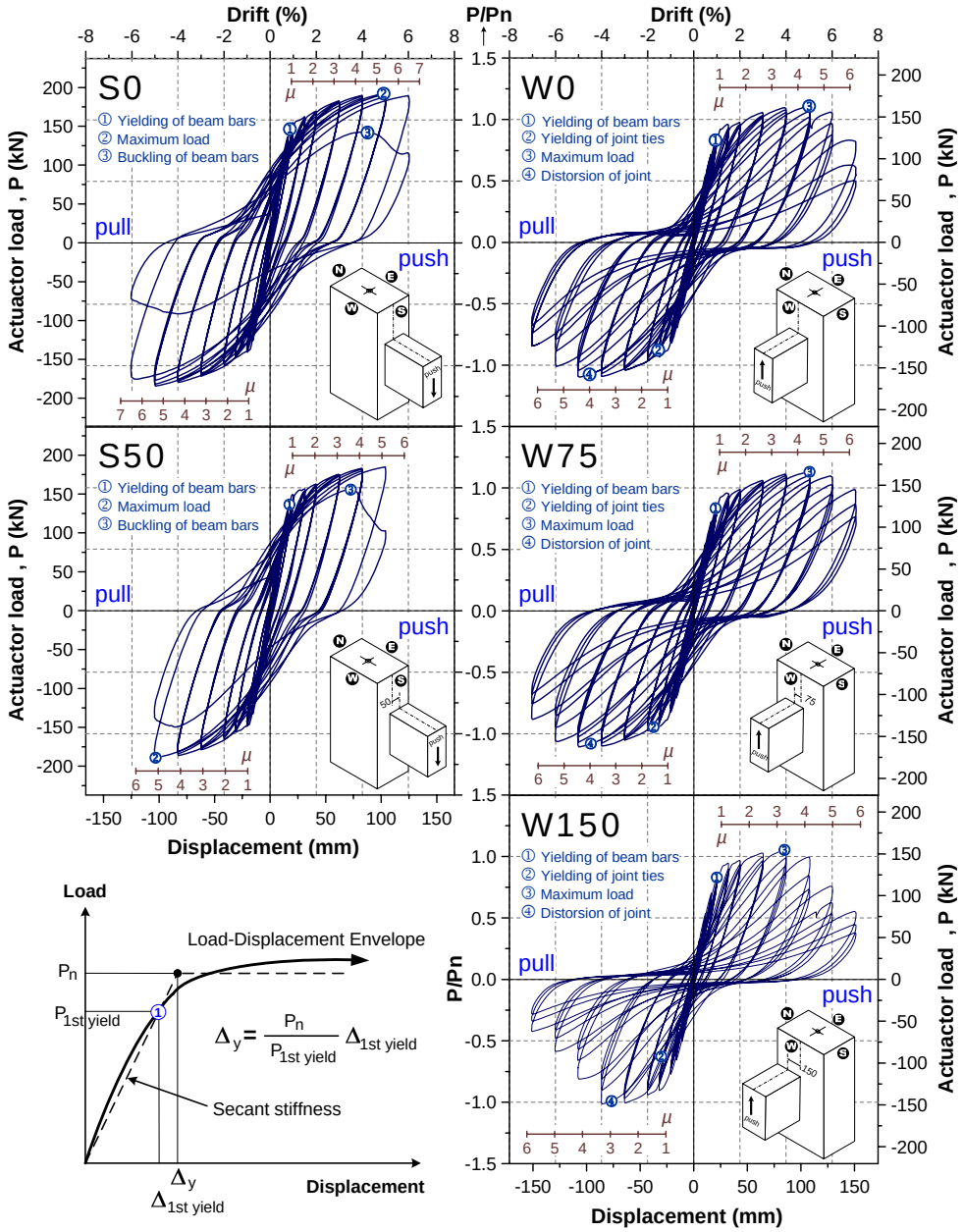

Figure 5 Load versus displacement response

Crack Development and Failure Modes

The failure mode of S-series specimens was classified as beam flexural failure (mode B) due to buckling of beam bars, while that of W-series specimens was classified as joint shear failure after beam flexural yielding (mode BJ). Figure 6 shows the final damage states and failure modes of two eccentric connections with flush beam-column faces. For the specimen S50 shown in Fig. 6(a), only hairline shear (diagonal) cracks were observed on the east (flush) face of the joint during testing. Concrete core crushing in the beam plastic region was evident, and only minor concrete cover spalling was observed on the east (flush) face of the joint adjacent to beam-column interfaces. Another concentric specimen S0 had similar damage progression. It was concluded that both joints could maintain integrity and remain elastic during the formation of the beam plastic hinge.

For the specimen W150 shown in Fig. 6(b), initial joint shear cracks diagonally appeared on the north face of the column during the 0.5% drift cycle, followed by propagation of the cracks up to 4% drift level. After strength degradation initiated at 4% drift, however, no new diagonal cracks appeared while crushing and spalling of concrete started on the north face of the joint. On the east face of the joint, flexural and torsional cracks first appeared during the 1.5% drift cycle, followed by extensive cracking due to a push-out compression from 90-degree hooks of the beam longitudinal bars. By the end of the test, severe crushing and spalling of concrete were evident on east, west, and north face of the column.

Visible damage observed in the other two W-series specimens was less than that observed in specimen W150. Due to distance between beam and column edges (Fig. 1), initial joint shear cracks diagonally appeared on the north face of the column during the 1.0% and 1.5% drift cycle for specimen W75 and W0, respectively. Concrete crushing was only observed on the west face of the joint adjacent to the beam-column interface. Extensive push-out cracks distributed on the east face of the joint, but concrete cover did not spall off during testing. (Ko 2005)

(a) Final damage state of specimen S50

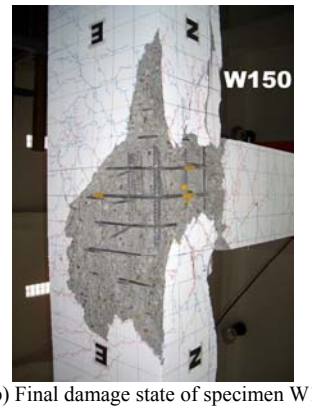

(b) Final damage state of specimen W150

Figure 6 Typical failure modes for test specimens

Energy Dissipation Capacity

As shown in Fig. 7, the relative energy dissipation ratio (β) and the equivalent viscous damping ratio (ξ_{eq}) are used to evaluate the performance level of the energy dissipation capacity for the test specimens. The first index β represents a fatter or narrower hysteretic curve (pinching effect) with respect to an elastic perfectly plastic model. Another quantitative index ξ_{eq} describes the hysteretic damping or energy dissipation pre cycle with respect to an equivalent linear elastic system.

Average β and ξ_{eq} of three cycles at each drift level for the test specimens are compared in Fig. 7(b) and 7(c). Three levels of energy dissipation capacity are evident. The flexure-dominated specimen S0 and S50 had best performance, while specimen W150 had worst performance. The performance of small-joint-eccentricity specimen S50 and W75 were inferior to that of concentric specimen S0 and W0, respectively. For the large-joint -eccentricity specimen W150, the joint deteriorated in a faster rate leading to worst performance.

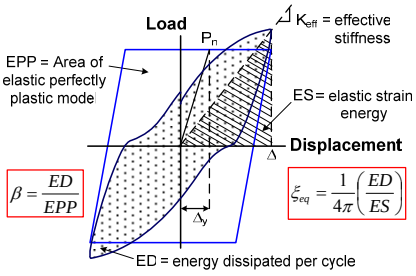

(a) Normalized index for energy dissipation capacity

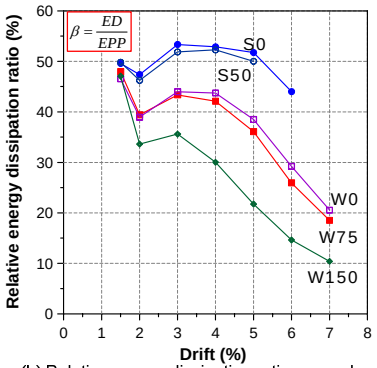

(b) Relative energy dissipation ratio per cycle

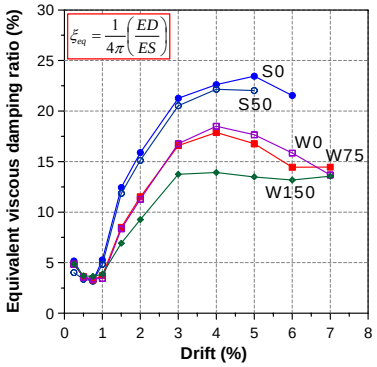

(c) Equivalent viscous damping ratio per cycle

Figure 7 Normalized energy dissipation at each drift level

Steel Strain Profiles

Strain gages were installed at selected positions on reinforcing bars before assembling into steel cages. Three layers of transverse reinforcement at spacing of 100 mm were placed in the joint for all specimens. Only the strain profiles for the central layer of joint hoops and crossties in W-series specimen was presented in Fig. 8. For corresponding drift ratios, the strains in the hoop legs on the exterior (north) side of the eccentric joints (specimen W75 and W150) were larger than those of the concentric joint (specimen W0). These profiles confirms the observations that more extensive shear or torsion cracks on the exterior side of the joint. On the interior (south) side, the strains in eccentric joints were less than those in concentric joint. For the W-series

specimen, yielding of crossties or hoop legs were recorded during 2% or 3% cycle. In contrast, the hoops and crossties in each direction for S-series specimen remained elastic to the end of test (Ko 2005).

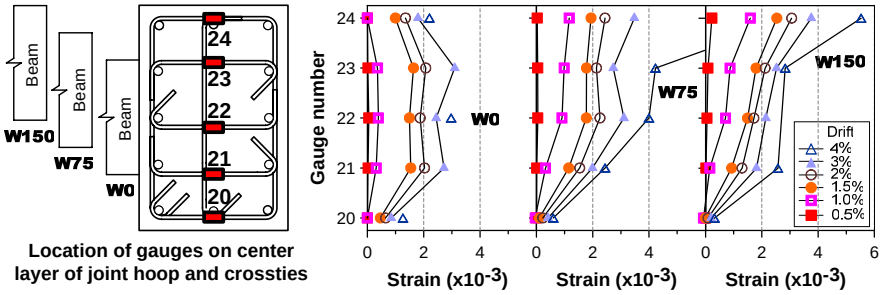

Figure 8 Strain profiles for the center layer of joint hoops and crossties in W-series specimens

Joint Shear Capacity

Three levels of strength and ductility ratios for the test specimens were shown in Table 3. Since the maximum loads of specimen S0 and S50 were govern by beam flexure rather than joint shear, S-series specimens had about 20% over strength and a ductility ratio greater than 5. In contrast, specimen W0 and W75 had about 10% over strength and a ductility ratio of 4.4 due to in-complete formation of beam plastic hinges. Finally, specimen W150 had only 3% over strength and a less ductility ratio of 3.3.

Corresponding to the measured maximum loads, the maximum joint shear acting on the joint was computed using equilibrium equations and standard moment-curvature analysis with measured material properties. Due to strain-hardening of reinforcing bars, the maximum input joint shear exceeded the design joint shear. As shown in Table 3, the maximum joint shear stress levels were calculated using Eqs.(1), (2), and (3). It should be noted that the three levels of joint shear stress calculated using Eq.(3) agree well with the three levels of seismic performance for the tested specimens. However, both equations in ACI Building Code (2005) and ACI 352 recommendations (2002) for estimating nominal joint shear strength were unconservative for the BJ failure mode.

Table 3 Test results

Specimen	S0	S50	W0	W75	W150
Nominal yield load P_n, kN	158	158	147	147	147
Nominal yield displacement Δ_y, mm	19.2	20.2	24.3	24.2	26.0
Over strength factor $P_{\max}/P_n$	1.22	1.20	1.11	1.12	1.03
Ductility ratio $\Delta_{\max}/\Delta_y$	5.31	5.12	4.43	4.47	3.32
Maximum joint shear $V_{jh,test}$, kN	828	789	775	780	710
Maximum shear stress level γ_{test} †	0.60 (0.68)	0.76 (0.65)	0.59 (0.79)	0.75 (0.80)	1.03 (0.91)
Failure mode‡	B	B	BJ	BJ	BJ

† $\gamma_{test} = V_{jh.test}/\sqrt{f_c'}\, b_j h_c$; values outside parentheses are computed using b_j^{318} as per Eq. (2), and values inside parentheses are computed using b_j^{352} as per Eq. (3).

‡Failure mode B means beam flexural failure; and BJ means joint shear failure after beam yielding.

CONCLUSIONS

Current ACI design provisions for estimating the joint shear strength of eccentric beam-column connections are established based on few experimental investigations of eccentric connections. The effects of column's aspect ratio and eccentric beam on joint shear strength are considered by the provisions of the effective joint width. Additional experimental verifications on the design provisions for eccentric connections are needed, particular in eccentric corner connections with rectangular columns. This paper presents experimental results of five corner connections with one concentric or eccentric beam framing into a rectangular column in strong or weak direction. Experimental results show that joint shear strengths in strong and weak direction of a rectangular column were very different. Two joints connecting a beam in strong direction were capable of supporting adjacent beam plastic mechanisms. The other three joints connecting a beam in weak direction, however,

exhibited significant damage and loss of strength after beam flexural yielding. Eccentricity between beam and column centerlines had detrimental effects on the strength degradation, energy dissipation capacity, and displacement ductility of the specimens. Valuable information is provided to help further improve the design requirements for eccentric corner beam-column connections.

REFERENCES

ACI Committee 318, (2005) *Building Code Requirements for Structural Concrete (ACI 318-05) and Commentary (ACI 318R-05)*, American Concrete Institute, Farmington Hills, Mich., USA.

ACI-ASCE Committee 352, (1976) "Recommendations for Design of Beam-Column Joints in Monolithic Reinforced Concrete Structures," *ACI JOURNAL*, Vol. 73, No. 7, pp. 375-393.

ACI-ASCE Committee 352, (1985) "Recommendations for Design of Beam-Column Joints in Monolithic Reinforced Concrete Structures," *ACI JOURNAL*, Vol. 82, No. 3, pp. 266-283.

ACI-ASCE Committee 352, (1991) "Recommendations for Design of Beam-Column Joints in Monolithic Reinforced Concrete Structures, (ACI 352R-91)" American Concrete Institute, Farmington Hills, Mich., USA.

ACI-ASCE Committee 352, (2002) "Recommendations for Design of Beam-Column Connections in Monolithic Reinforced Concrete Structures (ACI 352R-02)," American Concrete Institute, Farmington Hills, Mich., USA.

Burak, B., and Wight, J. K., (2002) "Seismic Behavior of Eccentric R/C Beam-Column-Slab Connections under Sequential Loading in Two Principal Directions," *ACI Fifth International Conference on Innovation in Design with Emphasis on Seismic, Wind and Environmental Loading, Quality Control, and Innovation in Materials/Hot Weather Concreting*, SP-209, V.M. Malhotra, ed., American Concrete Institute, Mich., pp. 863-880.

Chen, C. C., and Chen, G. K., (1999) "Cyclic Behavior of Reinforced Concrete Eccentric Beam-Column Corner Joints Connecting Spread-Ended Beams," ACI Structural Journal, V. 96, No. 3, pp. 443-449.

Joh, O., Goto, Y., and Shibata, T., (1991) "Behavior of Reinforced Concrete Beam-Column Joints with Eccentricity," *Design of Beam-Column Joints for Seismic Resistance*, SP-123, J. O. Jirsa, ed., American Concrete Institute, Farmington Hills, Mich., USA, pp. 317-357.

Ko, J. W., (2005) "Cyclic Tests of Reinforced Concrete Corner Beam-Column Joints with Eccentricity," master's thesis, Department of Construction Engineering, National Yunlin University of Science and Technology, Yunlin, Taiwan, also in the National Science Council Project Report No. NSC 93-2211-E-224-010, project supervisor Lee, H. J. (in Chinese)

Lawrance, G. M., Beattie, G. J., and Jacks, D. H., (1991) "The Cyclic Load Performance of an Eccentric Beam-Column Joint," *Central Laboratories Report* 91-25126, Central Laboratories, Lower Hutt, New Zealand.

Mander, J. B., Priestley, M. J. N. and Park, R., (1988) "Theoretical Stress-Strain Model for Confined Concrete," *Journal of the Structural Division*, *ASCE*, Vol. 114, No. 8, pp. 1804-1826.

Priestley, M. J. N., Seible, F., and Calvi, G. M., (1996) *Seismic Design and Retrofit of Bridges*, John Wiley and Sons, Inc., New York, USA.

Raffaelle, G. S., and Wight, J. K., (1995) "Reinforced Concrete Eccentric Beam-Column Connections Subjected to Earthquake-Type Loading," *ACI Structural Journal*, V. 92, No. 1, pp. 45-55.

Shin, M., and LaFave, J. M., (2004) "Seismic Performance of Reinforced Concrete Eccentric Beam-Column Connections with Floor Slabs, " *ACI Structural Journal*, Vol. 101, No. 3, pp. 139-148.

Teng, S., and Zhou, H., (2003) "Eccentric Reinforced Concrete Beam-Column Joints Subjected to Cyclic Loading," *ACI Structural Journal*, Vol. 100, No. 2, pp. 139-148.

Vollum, R. L., and Newman, J. B., (1999) "Towards the Design of Reinforced Concrete Eccentric Beam-Column Joints," *Magazine of Concrete Research*, V. 51, No. 6, 1999, pp. 397-407.